ELSEVIER

Journal of Alloys and Compounds 227 (1995) 180–185

Journal of ALLOYS AND COMPOUNDS

Hydrogenation of multicomponent Zr-base C15 type alloys

Y.-S. Hsu, T.-P. Perng

Department of Materials Science and Engineering, National Tsing Hua University, Hsinchu, Taiwan

Received 20 January 1995; in final form 20 March 1995

Abstract

A series of multicomponent Zr-base AB_2 alloys (Zr–Mn–Ni, Zr–Ti–Mn–Ni, Zr–Mn–V–Ni, and Zr–Mn–V–Co–Ni) were prepared. The major phase in the alloys had a C15-type structure with the lattice parameter varying with the atomic radii of A and B atoms. Absorption and desorption of hydrogen gas were performed in a Sievert's apparatus. The kinetics of the first few cycles of hydriding–dehydriding was collected. The P–C–T curves were also established for these alloys. It was found that these kinetic and thermodynamic properties were highly dependent on the solid solution in atomic site of A or B. The hydrogenation properties are explained based on the composition, the alloying element, and the free cell volume of the alloys.

Keywords: Metal hydrides; C15 Laves phase; Zr-base alloy; Hydrogenation

1. Introduction

In the past 30 years, a lot of effort has been put into studying the fundamental properties of metal hydrides for hydrogen storage and transport applications. Several alloy systems, such as AB_5-type alloys based on $LaNi_5$ [1–3], and AB_2-type alloys, known as the Laves phase alloys [4–9], have been extensively studied.

Being an important group of size-factor intermetallic compounds, Laves phases are obtained by alloying two elements whose atomic radii, r_A and r_B, are in the ratio 1.1 to 1.6 [10]. The approximate formula is termed AB_2. They are close-packing, with three possible structure types, i.e., C15, C14, and C36, based on the crystal structures of $MgCu_2$, $MgZn_2$, and $MgNi_2$, respectively. The secret of the close relationship among these three structures is that the small atom B is arranged on the corners of tetrahedra. Different ways of joining such tetrahedra lead to various structures. The detailed crystallographic data are given elsewhere [10]. Such arrangement provides a large interstitial space and therefore accounts for a large hydrogen absorption capacity.

Besides the geometric factors, the electronic effects should also be taken into account to demonstrate the stability of Laves phases. Some authors [11] have proposed that there is a correlation between the averaged number of outer electrons (ANOE) and the structure type. For example, if the ANOE is smaller than 4.67, no Laves phase is formed. If the ANOE is between 4.67 and 5.4, Zr-base AB_2 alloys would exist as a C15-type structure but no Laves phase is formed in the Ti-base alloys. The C14-type structure appears to occur in Zr- and Ti-base alloys if the ANOE is between 5.4 and 7. When the ANOE is larger than 7, both of them form the C15-type structure again.

The hydrogen absorption–desorption properties of the Laves phase alloys could be modified through participation of foreign atoms. It has been proposed that the degree of hydrogenation depends on the d-electron concentration [12]; and the free cell volume and the binding energy between hydrogen and the hydride former (Ti or Zr) can influence the absorption capacity and the plateau pressure [13].

In this study, a series of Zr-base AB_2 alloys were prepared. The phase structures were identified. The gas-phase hydrogenation properties were examined and compared. The different characteristics are explained based on the composition and physical and chemical properties of the constituent elements, and the free cell volume of the alloys. These data are to be used to evaluate their electrochemical performance, to be presented in a subsequent paper.

SSDI 0925-8388(95)01646-5

2. Experimental

The alloys were prepared by mixing appropriate amounts of constituent elements (purity 99.9–99.99%) and by arc melting in an argon atmosphere. The ingots were turned over and remelted five or six times to ensure homogeneity. Seven alloys with the following compositions were investigated: $ZrMn_{0.6}Ni_{1.4}$, $ZrMn_{0.8}Ni_{1.2}$, $ZrMn_{0.6}V_{0.2}Ni_{1.2}$, $(Zr_{0.8}V_{0.2})Mn_{0.6}Ni_{1.4}$, $(Zr_{0.8}Ti_{0.2})Mn_{0.6}Ni_{1.4}$, $(Ti_{0.8}Zr_{0.2})Mn_{0.6}Ni_{1.4}$, and $ZrMn_{0.6}V_{0.2}Co_{0.1}Ni_{1.2}$. The alloy $ZrMn_{0.6}Ni_{1.4}$ was employed as a prototype composition.

Approximately 5 wt.% excess Mn was added to compensate for its high evaporation loss in the arc-melting process. Each ingot was then sealed in a quartz tube under vacuum and annealed at 1000°C for 10 h, followed by furnace cooling.

The alloy ingots were very brittle. They were pulverized into powders with a mechanical attritor under an argon atmosphere. X-ray diffraction (XRD) analysis was used to check whether the C15-type Laves phase was obtained. Silicon powder was added as an internal standard. The lattice constants were then determined.

Powders between 100 and 325 mesh were selected for hydrogen absorption and P–C–T measurements. Approximately 5 grams of powder were loaded into a stainless steel reactor in a volumetric system which has been previously described [14]. The sample powder was activated at 400°C and 1 MPa of hydrogen gas for 30 min, then cooled down to room temperature. Hydrogen gas at 3.3 MPa was introduced into the system for the kinetics study. After several cycles of hydriding and dehydriding, the powder was completely dehydrided at 400°C before the P–C–T isotherm measurement was conducted.

3. Results and discussion

3.1. Phase identification

The XRD patterns of all the alloys are shown in Fig. 1. It was found that most of them, except for $(Ti_{0.8}Zr_{0.2})Mn_{0.6}Ni_{1.4}$, exhibited similar features. The main diffraction peaks were ascribed to (220), (311), and (222); and they were indexed as face-centered cubic C15-type Laves phase. For $(Ti_{0.8}Zr_{0.2})Mn_{0.6}Ni_{1.4}$, the major phase had a C14-type structure. It is interesting to note that $ZrMn_2$ is classified as a C14-type Laves phase, while no distinct structure type can be assigned for $ZrNi_2$ [13]. However, alloys prepared based on these two compositions, $ZrMn_{0.6}Ni_{1.4}$ and $ZrMn_{0.8}Ni_{1.2}$, exhibited the C15-type structure.

The ANOE for the Zr-base alloys prepared here varied from 7.07 to 7.47, and were predicted to form a C15-type structure [13]. The Ti-base compound with this range of ANOE would not form any stable C15-type structure. Our result for $(Ti_{0.8}Zr_{0.2})Mn_{0.6}Ni_{1.4}$ showed that C14-type structure was the major phase.

Based on the prototype composition, $ZrMn_{0.6}Ni_{1.4}$, modifying the composition could retain the phase structure but cause a lattice distortion. The lattice constants for the C15-type alloys were determined from the three main peaks. They are plotted in Fig. 2 for comparison. Structure expansion or contraction takes place due to the partial substitution or addition of the alloying elements. Expansion of the structure would give a larger free cell volume for absorbing hydrogen and vice versa.

For these alloys, optical metallographic examination showed that there was some minor second phase dispersed in the matrix phase, although the XRD patterns could hardly detect the presence of the second phase.

3.2. Hydrogen absorption kinetics and P–C–T isotherms

The results of hydrogen absorption kinetics and P–C–T isotherms for the above seven alloys are

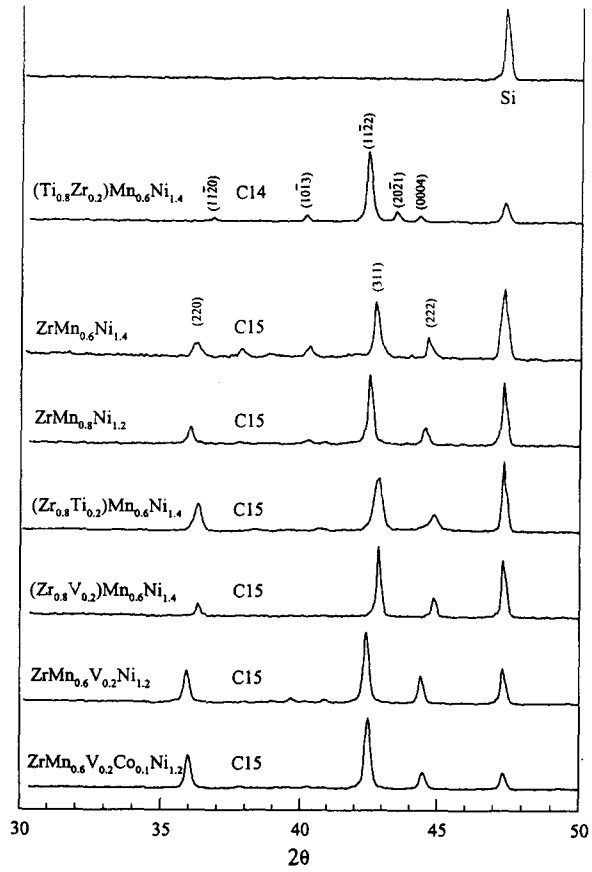

Fig. 1. X-ray diffraction patterns of the alloys. Si is used as an internal standard.

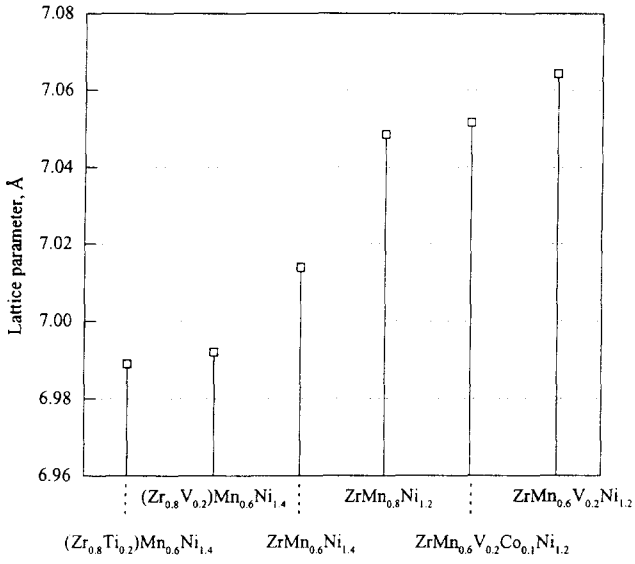

Fig. 2. Lattice parameters of the C-15-type alloys.

reported and compared in this section. In general, the Zr-base C15-type intermetallic compounds had a high hydrogen absorption rate and tended to form a flat plateau. The plateau pressure and the hydrogen storage capacity were affected by the substitution or addition of different alloying elements. Hysteresis was always observed in each curve. These results could be explained in terms of the atomic size and the hydriding property of the alloying elements. Table 1 lists some characteristics of the selected elements, including lattice structure, atomic radius, hydride formation enthalpy, and some selected physical and chemical properties. These data serve as the basis to interpret the following experimental results.

3.2.1. Effect of substitution of Ni with Mn

Two alloys, $ZrMn_{0.6}Ni_{1.4}$ and $ZrMn_{0.8}Ni_{1.2}$, were compared to examine the effect of substitution of Ni with Mn. Their absorption kinetics curves, along with those for other alloys, are shown in Fig. 3. The equilibrium pressure of the first cycle was always lower than those in the second and the third cycles. This indicated that there was some irreversible hydrogen trapped in the first cycle so that the alloy absorbed less

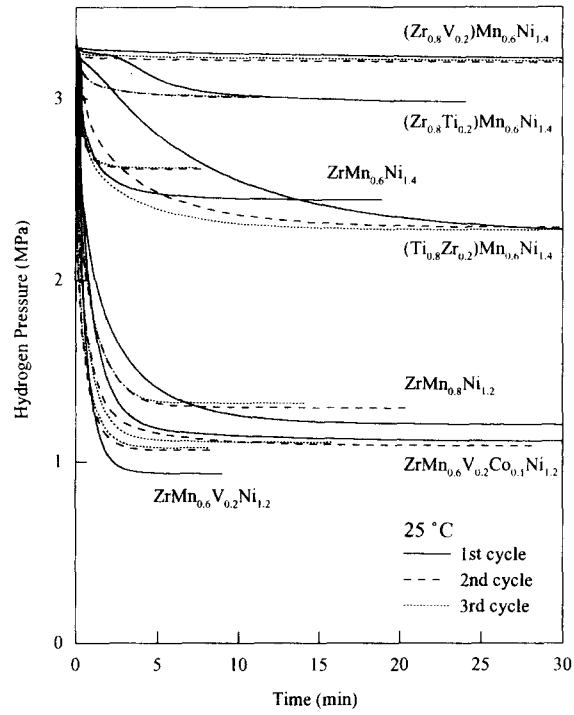

Fig. 3. Hydrogen absorption kinetics curves for the alloys at 25°C.

Table 1
Selected physical and thermodynamic data for the alloying elements

Element	Ti	Zr	Mn	V	Co	Ni
Atomic weight ($g\ mol^{-1}$)	47.88	91.22	54.94	50.94	58.93	58.69
Atomic radius[a] (Å)	1.45	1.59	1.36	1.31	1.25	1.24
Structure type	{hcp[bcc]}[b]	{hcp[bcc]}	cubic	bcc	[hcp/fcc][c]	fcc
Melting point (°C)	1667	1852	1244	1902	1495	1453
Latent heat of sublimation at 25 °C ($kJ\ mol^{-1}$)	469.3	612.1	291.0	510.2	425.0	429.6
Enthalpy of hydride formation at 25 °C[d]	TiH_2	ZrH_2	$MnH_{0.5}$	$VH_{0.5}$	$CoH_{0.5}$	$NiH_{0.5}$
(kJ per mol H)	−68	−82	−8	−35	+15	−3
Properties	hard, corrosion resistant	hard, corrosion resistant	white, brittle, reactive	hard, corrosion resistant	hard, gray color	quite corrosion resistant

[a] Estimated from M–M bond length, obtained from CRC *Handbook of Chemistry and Physics*, 72, 9–1.
[b] hcp is stable at room temperature; bcc exists when T is above the phase transition temperature.
[c] Mixed structure of ...ABCABABCAB... .
[d] From Ref. [16].

hydrogen in the subsequent cycles. Continuous activation took place during the first three cycles. Therefore some microcracks continually formed and newly activated surfaces were continuously produced. This led to increased absorption rates in the second and the third cycles, and the equilibrium hydriding capacity was soon achieved after a few absorption–desorption cycles. The final equilibrium pressure of $ZrMn_{0.8}Ni_{1.2}$ was found to be much lower than that of $ZrMn_{0.6}Ni_{1.4}$.

The P–C–T curves for these two alloys, along with other alloys to be presented in the subsequent sections, are compared in Fig. 4. They both tended to form flat plateaus. Since the maximum pressure employed in the absorption experiment was 5.1 MPa, the curve for $ZrMn_{0.6}Ni_{1.4}$ was not completed. The dotted segment is used to illustrate the difference of equilibrium pressure between the absorption and desorption processes. It also seemed that $ZrMn_{0.6}Ni_{1.4}$ decomposed, since the isotherm did not close for the desorption. For $ZrMn_{0.8}Ni_{1.2}$, the plateau pressures were lower compared with those of $ZrMn_{0.6}Ni_{1.4}$. This can be derived from the kinetic study, as observed in Fig. 3. It was noted that there existed a large hysteresis between the absorption and desorption plateau for both alloys. Park et al. [15] have found that $ZrMn_2$-base intermetallic compounds usually possess a large hysteresis energy, expressed as $(1/2)RT\ln(P_a/P_d)$, where P_a is the absorption plateau pressure, and P_d is the desorption plateau pressure. The presence of hysteresis causes an efficiency loss in thermodynamic performance, and is a drawback for application of hydrides in heat pumps or in Ni-hydride batteries. Park et al. [15] also observed that ZrV_2-based alloys had the lowest hysteresis, based on the strain energy viewpoint. This led us to add some vanadium to these alloys to study its effect on the hydrogenation properties.

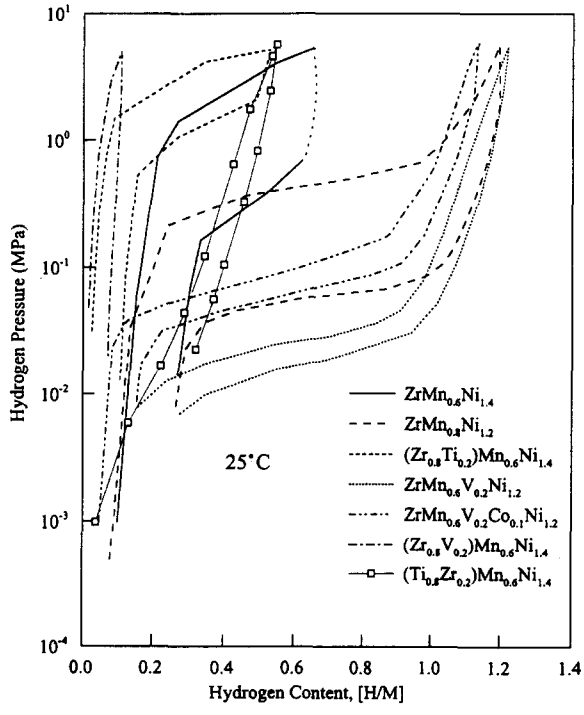

Fig. 4. The P–C–T isotherms for the alloys at 25°C.

3.2.2. Effect of substitution of Mn or Zr with V

The formation enthalpy of $VH_{0.5}$ at 25°C is −35 kJ per mol H [16]. This value is larger than those of Mn (−8 kJ per mol H for $MnH_{0.5}$) and Ni (−3 kJ per mol H for $NiH_{0.5}$). However, it is smaller than those of Ti and Zr (−68 kJ per mol H for TiH_2, and −82 kJ per mol H for ZrH_2) [16]. The position of V in the AB_2 Laves phase alloy is uncertain. Based on the phase diagrams [17], there is an unlimited mutual solubility for Ti and Zr at room temperature. Vanadium, in contrast, has only a limited solubility in both Ti and Zr. Thus, two pairs of alloys, $ZrMn_{0.8}Ni_{1.2}$ versus $ZrMn_{0.6}V_{0.2}Ni_{1.2}$, and $(Zr_{0.8}V_{0.2})Mn_{0.6}Ni_{1.4}$ versus $ZrMn_{0.6}Ni_{1.4}$, were examined to explore the effect of substitution of Mn or Zr with V.

The partial substitution of V on the B site was checked first. The absorption kinetics curves for $ZrMn_{0.8}Ni_{1.2}$ and $ZrMn_{0.6}V_{0.2}Ni_{1.2}$ shown in Fig. 3 are compared. As $ZrMn_{0.6}V_{0.2}Ni_{1.2}$ had the largest lattice expansion, as was seen in Fig. 2, and V is a stronger hydride former than Mn and Ni, its equilibrium pressure is anticipated to be lower. Furthermore, it also displayed a relatively higher absorption rate. Thus V on the B site could greatly improve the hydrogen absorption capacity and kinetics. From the P–C–T isotherms, Fig. 4, it was seen that the maximum hydrogen content [H/M] of this alloy was larger than that of $ZrMn_{0.8}Ni_{1.2}$, and was the largest among all compositions studied here. In addition, the plateau pressure was found to be the lowest and the hysteresis loop was greatly reduced.

If the A sites were partially occupied by V, the kinetics curves shown in Fig. 3 indicated a totally different consequence. The alloy $(Zr_{0.8}V_{0.2})Mn_{0.6}Ni_{1.4}$ hardly absorbed any hydrogen. From the previous XRD analysis, a C15-type Laves phase pattern and a lattice shrinkage with respect to $ZrMn_{0.6}Ni_{1.4}$ were observed for this alloy. A very steep P–C–T curve is displayed in Fig. 4. Therefore, it seems that V is better categorized as a B-site alloying atom in the AB_2 alloy for practical applications.

3.2.3. Effect of substitution of Zr with Ti

In this section, four alloys, $ZrMn_{0.6}Ni_{1.4}$, $(Zr_{0.8}V_{0.2})Mn_{0.6}Ni_{1.4}$, $(Zr_{0.8}Ti_{0.2})Mn_{0.6}Ni_{1.4}$, and $(Ti_{0.8}Zr_{0.2})Mn_{0.6}Ni_{1.4}$, are to be compared. There are some similarities between Zr and Ti. First of all, they both have a stable hcp structure at room temperature and a bcc structure at higher temperatures (above

882°C for Ti and 852°C for Zr). As mentioned previously, they dissolve in each other completely at any composition and they both form stable hydrides. From the economics point of view, it is desirable to replace Zr by Ti as much as possible.

As was seen in Fig. 2, the most severe structure contraction in these C15-type alloys occurred in $(Zr_{0.8}Ti_{0.2})Mn_{0.6}Ni_{1.4}$. It was expected that the hydrogen absorption ability of this alloy would be worse than that of $ZrMn_{0.6}Ni_{1.4}$. The results shown in Fig. 3 confirmed this prediction. Nevertheless, the performance of this alloy was still better than that of $(Zr_{0.8}V_{0.2})Mn_{0.6}Ni_{1.4}$. The P–C–T curves shown in Fig. 4 also displayed a similar result. This could be explained in terms of the different formation enthalpies of TiH_2 and $VH_{0.5}$. Titanium might have helped keep hydrogen in the alloy even though more shrinkage accompanied the addition of Ti. Although the plateau pressure of $(Zr_{0.8}Ti_{0.2})Mn_{0.6}Ni_{1.4}$ was higher in comparison with that of $ZrMn_{0.6}Ni_{1.4}$, reduction in the hysteresis loss and decrease in the amount of irreversible hydrogen were found in the P–C–T curve.

For $(Ti_{0.8}Zr_{0.2})Mn_{0.6}Ni_{1.4}$, its XRD pattern showed a totally different feature from those of other alloys in this experiment. The major peaks could be classified as a C14-type Laves phase. From Fig. 3, a slower absorption rate but a lower final equilibrium pressure were found for this alloy when compared with those of $ZrMn_{0.6}Ni_{1.4}$. A sloped "plateau" was observed in its P–C–T isotherm (Fig. 4). It is proposed that the hydrogen absorption behavior is strongly structure dependent, even though Zr is a stronger hydride former than Ti. It was also noted that both of the Ti-containing alloys, $(Zr_{0.8}Ti_{0.2})Mn_{0.6}Ni_{1.4}$ and $(Ti_{0.8}Zr_{0.2})Mn_{0.6}Ni_{1.4}$, showed much slower absorption kinetics in the first cycle (Fig. 3). They exhibited slower activation in the initial hydrogenation.

3.2.4. Effect of addition of Co

From a practical standpoint, alloys possessing a superior absorption–desorption characteristic at around 1 atm are better candidates for applications at ambient condition. Based on the preceding discussion, the distinctive structure of Laves phase intermetallic compounds could be retained by proper substitution with some elements. The modified compounds could alter hydrogen absorption–desorption properties. Until now, it has been observed that the composition $ZrMn_{0.6}V_{0.2}Ni_{1.2}$ had excellent features such as massive storage, fast absorption, and small hysteresis on hydrogenation. However, the plateau pressure was well below 1 atm (0.1 MPa) at 25°C. To some extent, the hydride was too stable and a discount of the efficiency on the utilization of the reversible hydrogen remained a concern. To raise the plateau pressure, Co was recommended because of the positive formation enthalpy of $CoH_{1.5}$ (+ 15 kJ per mol H) [16]. Furthermore, it was also desirable to explore the stoichiometric limit of AB_2-type alloys. For this reason, Co was added to the B site, and comparison of $ZrMn_{0.6}V_{0.2}Co_{0.1}Ni_{1.2}$ and $ZrMn_{0.6}V_{0.2}Ni_{1.2}$ was carried out.

From Figs. 1 and 2, the XRD pattern of $ZrMn_{0.6}V_{0.2}Co_{0.1}Ni_{1.2}$ indicated that the C15-type structure was preserved, and a lattice expansion was generated. The hydrogen absorption kinetics curves of these two alloys are compared in Fig. 3. It was seen that the performance on the absorption rate and storage capacity of the Co-added alloy was just a little poorer in comparison with that of $ZrMn_{0.6}V_{0.2}Ni_{1.2}$. However, the plateau pressure, as shown in Fig. 4, was raised to around 1 atm and the amount of irreversible hydrogen was reduced. This demonstrated that the above theories employed to explain the hydrogenation properties for C15-type alloys could also be applied to this five-component alloy. The optimum gas-phase hydrogenation property of this alloy would lead to a better electrochemical performance for Ni-hydride battery application, which will be presented in a separate paper.

4. Conclusions

1. The Zr–(Mn–Ni) based AB_2 Laves phase intermetallic compounds studied here had the C15-type cubic structure. The structure correlated with the ANOE values of the alloys. By proper substitution or addition of foreign elements, the alloys could still retain the structure, except that lattice expansion or contraction occurred. The hydrogenation kinetics, plateau pressure, absorption capacity, and hysteresis could also be modified.

2. Substitution of Ni by Mn on the B site tended to lower the plateau pressure and to form a flatter plateau, but was accompanied by a larger hysteresis.

3. Vanadium might occupy the A or B site. When the B-site atoms were partially substituted with V, the hydrogen absorption rate and capacity were greatly increased, and the hysteresis was greatly reduced, but the plateau pressure was lower than 1 atm at 25°C. When it partially replaced Zr on the A site, a severe structure shrinkage was induced. Absorption of hydrogen was significantly hindered.

4. When Ti partially replaced Zr on the A site, it caused a structure contraction. The plateau pressure was raised. The absorption capacity became smaller, but both the hysteresis and the amount of irreversible hydrogen were slightly reduced. When more Zr was replaced by Ti, a new phase structure, C14-type hexagonal Laves phase, evolved. The hydrogen ab-

sorption behavior was very much different from those of other C15-type alloys.

5. Addition of some cobalt still maintained the Laves phase structure. The hydrogenation behavior could be modified to meet the required application.

Acknowledgments

This work was supported by the National Science Council of Republic of China under Contract NSC 83-0405-E-007-013 and National Tsing Hua University Fellowship 82-2-1.

References

[1] G. Bronoel, J.C. Achard and L. Schlapbach, *Int. J. Hydrogen Energy, 1* (1976) 251.
[2] T.Sakai, H. Miyamura, N. Kuriyama, A. Kato, K. Oguro and H. Ishikawa, *J. Electrochem. Soc., 137* (1990) 795.
[3] P.H. L. Notten and P. Hokkeling, *J. Electrochem. Soc., 138* (1991) 1877.
[4] D. Shaltiel, I. Jacob and D. Davidov, *J. Less-Common Met., 53* (1977) 117.
[5] Y. Moriwaki, T. Gamo, A. Shintani and T. Iwaki, *Denki Kagaku, 57* (1989) 488.
[6] T. Gamo, Y. Moriwaki, N. Yanagihara, T. Yamashita and Y. Iwaki, *Int. J. Hydrogen Energy, 10* (1985) 39.
[7] Y. Moriwaki, T. Gamo, H. Seri and T. Iwaki, *J. Less-Common Met., 172* (1991) 1211.
[8] K. Sapru, K. Hong, M.A. Fetcenko and S. Venkatesan, U.S. Patent 4,551,400, 1985.
[9] M.A. Fetcenko, U.S. Patent 5,002,730, 1991.
[10] K. Girgis, in R.W. Cahn and P. Haasen (eds.), *Physical Metallurgy*, Amsterdam, New York, 3rd edn., 1983, p. 240.
[11] R.P. Elliot and W. Rostocker, *Trans. ASM, 50* (1958) 617.
[12] J.J. Reilly, *Int. Symp. on Hydrides for Energy Storage, Geilo, Norway, Aug., 1977*, p. 527.
[13] O. Bernauer, J. Topler, D. Noreus, R. Hempelmann and D. Richter, *Int. J. Hydrogen Energy, 14* (1989) 187.
[14] S.-M. Lee and T.-P. Perng, *J. Alloys Comp., 177* (1991) 107.
[15] J.-M. Park, Y.-G. Kim and J.-Y. Lee, *J. Alloys Comp., 198* (1993) L19.
[16] R. Griessen and T. Riesterer, in L. Schlapbach (ed.), *Hydrogen in Intermetallic Compounds I*, Springer-Verlag, Berlin, 1988, p. 266.
[17] ASM Handbook, *Alloy Phase Diagrams*, Vol. 3, ASM International, Materials Park, OH, 1992.